

# Interpreting the Therapeutic Efficiency of Multifunctional Hybrid Nanostructure against Glioblastoma

Zemin Ou,<sup>‡</sup> Xinjian Li,<sup>‡</sup> Yun You, Dewen Liu,<sup>\*</sup> and Jinyu Wang<sup>\*</sup>Cite This: *ACS Omega* 2023, 8, 12259–12267

Read Online

ACCESS |



Metrics &amp; More

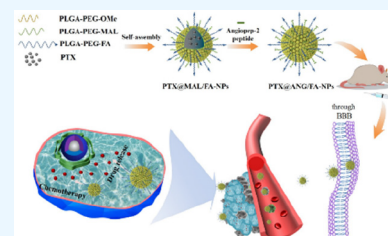


Article Recommendations



Supporting Information

**ABSTRACT:** Glioblastoma is considered the most fatal malignant brain tumor that starts from the central nervous system (CNS), where the blood–brain barrier (BBB) remains the biggest challenge for active targeting of drugs in malignant brain tumor. Thereby, we have designed a paclitaxel PTX@ANG/FA-NPs hybrid novel nanodrug delivery system that can overcome the clinical BBB. The structural and morphological characterization of PTX@ANG/FA-NPs confirmed successful synthesis of nanomicelles with the size range of about 160 to 170 nm. The overall repressive effect of PTX@ANG/FA-NPs on human glioblastoma U251 cells was 1.2-times that of PTX alone. *In vitro* cellular uptake assay also demonstrated that the dual-targeted nanoparticles (NPs) were more easily taken up by glioblastoma U251 cells. Although the antiglioblastoma activity was confirmed by cell migration assay, apoptosis assay, and cellular uptake assay, the absorption was studied by *in vivo* fluorescence imaging and brain distribution. The synthesized PTX@ANG/FA-NPs probe significantly inhibited the migration of U251 within the cells and promoted the apoptosis process. Moreover, the RhB@ANG/FA-NPs and PTX@ANG/FA-NPs showed higher accumulating potential at sites of tumor BBB disruption. The novel nanodrug delivery system mediated enhanced distribution of drugs at the targeted site for therapeutics efficacies against glioblastomas across the BBB.



## 1. INTRODUCTION

Glioblastoma is a belligerent mode of cancer that develops in different parts of the brain. It can start at any stage of life but more often in older individuals. It causes worsening headaches, nausea, vomiting, and seizures that collectively account for about 57% of all kinds of gliomas and 48% of all initially malignant central nervous system (CNS) tumors.<sup>1,2</sup> In this case, the patients with brain tumors have no longer to survive than 16 months despite the combination of surgical and nonsurgical methods.<sup>3</sup> Glioblastomas have a perceptible malignant proliferative capacity, a high infiltrative competence, and a greater incidence of recurrence.<sup>4,5</sup> These types of tumors are located mainly in the brain parenchyma, are infiltrative, and grow diffusely. Precisely, the lack of histological boundaries that could be distinguished by the naked eye has made diagnostic complications in which surgery cannot fully remove the glioblastomas and lower the therapeutic efficacies.<sup>6,7</sup> Therefore, for these diseases, precise drug treatment is considered the best choice. However, the biggest difficulty with drug therapy is the blood–brain barrier (BBB) that comprises novel vascular structure consisting of multiple layers: brain endothelial cells layer and a highly selective, semipermeable chemical barrier that isolates the CNS from the peripheral tissues.<sup>8,9</sup> The major concern of the BBB is to reduce the free flow of biofluid concerning the blood toward the brain. On one edge, the BBB has very challenging tasks including regulation of transporters with respect to their permeability of molecules,<sup>10–12</sup> transportation of ions, providing nutrients in accordance with the neuron requirements, while on the other edge, this barrier

maintains homeostasis in the CNS by regulating materials and providing shelter to the neural tissue from pathogens and neurotoxic substances.<sup>13–16</sup> It also balances the majority of small-molecule drug candidates and provides 100% check for large-molecule drugs. Further, the permeability of the BBB is a rate-limiting factor for drug penetration into the CNS as a majority of effective chemotherapy drugs could not cross the BBB.<sup>17,18</sup> Therefore, certain encapsulation strategies are applied over the drugs to form an efficient nanodelivery system that can pass the BBB without side effects and improved bioavailability.<sup>19,20</sup> Such carriers prove safe delivery without harmful effects and at a considerably smaller dosage.<sup>21,22</sup>

Polyester poly(lactic-co-glycolic acid) (PLGA) is an effective constituent of poly lactic acid (PLA) and poly glycolic acid (PGA). The structure is fully biodegradable and capable of self-assembling into diverse form and size that can accommodate molecules of any size.<sup>23,24</sup> Many kinds of block copolymers made of polyesters together with poly ethylene glycol (PEG) were developed, which provided blockage and reduction of extraneous molecules with steric and hydrated repulsion and stability.<sup>25,26</sup> PEG–PLGA is not easily recognized by the

Received: December 30, 2022

Accepted: March 9, 2023

Published: March 22, 2023



immune system, but it extends the circulation time in the body and solves major problems of PLGA including poor solubility in water and easy clearance by the liver and spleen.<sup>27,28</sup> But PEG–PLGA has the same problem with a majority small-molecule chemotherapy drugs while crossing the BBB. Thereby, we designed an elaborate dual-targeting carrier that includes Angiopep-2 (ANG) and folate to solve this challenging task. ANG is a short low-density lipoprotein receptor-related protein-1 (LRP1)-binding peptide, consisting of 19 amino acid residues, and LRP1 is highly expressed in the endothelial cells of the brain capillary and the glioblastoma. Nanoparticles (NPs) modified by ANG showed to penetrate through the BBB and targeted glioma cells successfully.<sup>29</sup> To enhance the targeting effect of the carrier on glioblastoma, we also modified the surface of the carrier with folate. Since folate-carrier materials have the ability to bind to highly expressed folate receptors on the surface of glioblastoma, a PLGA-based dual targeting system containing folate and lactoferrin had been shown for targeting glioblastoma.<sup>30</sup> However, ANG demonstrated a substantially higher ability for transcytosis across bovine brain endothelial cells than lactoferrin, transferrin, and avidin.<sup>31</sup>

Paclitaxel (PTX) is active and effective chemotherapeutic molecule commonly used for a broad range of diseases, together with Adriamycin and cisplatin, as it is a first- or second-line treatment for diverse forms of cancer.<sup>32,33</sup> It functions by stabilizing microtubules, thereby blocking cell mitosis, making cancer cells unable to divide effectively, and eventually leads to death. However, the solubility of PTX is lower than 0.03 g/L, so its application has been severely limited by poor water solubility and rapid elimination.

In this research, PTX can be encapsulated into ANG/FA/PLGA nanoparticles, and the drug transport system can overcome the disadvantages of PTX such as the deprived water solubility, reduced bioavailability, and active targeting through the BBB. An important application of this study is to facilitate the efficient delivery of drugs and biological therapeutics toward brain and CNS diseases.

## 2. EXPERIMENTAL PROCEDURE

**2.1. Materials.** All the materials were purchased from multinational companies and up to standard; details are mentioned in the [Supporting Information](#).

**2.2. Cell Lines and Animals.** Glioblastoma U251 cells, Human cervical—a kind of cancer HeLa cells, and lung cancer A549 cells were obtained from the Cell Bank, which is a kind of Culture Collection in Chinese Academy of Sciences (Shanghai, China).

Male BALB/c-nu mice having weight of 22–25 g were part of current study and were kept at a temperature of  $22 \pm 3$  °C with continued 12 h light/dark cycle. All animals were given by the Peking University School of Medicine (Beijing, China). The study followed the rules and regulations from the ethical committee and Guidance of National Institutes of Health with maintenance of the laboratory animal's protocol.

**2.3. Preparation of ANG/FA/PLGA Nanoparticles.**  
**2.3.1. Preparation of Mal/FA-NPs and ANG/FA-NPs.** FA-targeted PLGA nanoparticles (NPs) were prepared with the emulsion solvent evaporation method. The PLGA–PEG–Mal, PLGA–PEG–Me, and PLGA–PEG–FA were dissolved in dichloromethane to obtain solution A. The sodium cholate solution was added to the solution A to obtain solution B, the solution B was filtered through a 0.22  $\mu\text{m}$  membrane after ultrasonic treatment with an ultrasonic cell disruptor (JY88–

IIN, HUXI, China) at 100 W power for 1 min, and the Mal/FA-NPs were obtained. The ANG was dissolved in the solution of Mal/FA-NPs at 25 °C using a magnetic stirrer at 310 rpm for 6 h, and the ANG/FA-NPs were obtained.

**2.3.2. Preparation of PTX@ANG/FA-NPs and RhB@ANG/FA-NPs.** The preparation method of PTX@ANG/FA-NPs and RhB@ANG/FA-NPs was the same as that of ANG/FA-NPs, and they were only slightly different in composition. The PTX@ANG/FA-NPs contained PTX, while RhB@ANG/FA-NPs contained RhB.

**2.4. Characterization of ANG/FA/PLGA NPs.**  
**2.4.1. The Tyndall Effect.** The RhB@Mal/FA-NPs were characterized under laser-beam irradiation to observe whether a bright “channel” appeared in the ANG/FA-NPs solution, presenting the Tyndall effect.

**2.4.2. ANG/FA/PLGA Nanoparticle Size and Zeta Potential.** Malvern laser instruments particle size analyzer (Malvern ZS 90, Malvern Instruments, UK.) was processed to examine the size and zeta potential of unique and novel dual-targeted RhB@Mal/FA-NPs and PTX@ANG/FA-NPs, which were enhanced into the vessel and the dimensions were carried out in triplicate after equilibrating at 25 °C for 30 s.

**2.4.3. ANG/FA/PLGA NPs Morphology.** Transmission electron microscopy (TEM) is an imperative tool for characterizing nanomaterial morphology. After drying at room temperature, the copper mesh was negatively stained with phosphotungstic acid for 30 s. The morphology of the PTX@ANG/FA-NPs was observed under TEM.

**2.4.4. Differential Scanning Calorimetry (DSC).** Taking 1 mL of 5 mg mL<sup>-1</sup> solution of FA-NPs, and dual-targeted PLGA nanocarriers (ANG/FA-NPs) separately, measuring with differential scanning calorimeter (Nano DSC, TA Instruments, USA), the initial temperature was set to 10 °C, and the final temperature was set to 130 °C. Pressure perturbation calorimetry (PPC) was performed at 3 Pa, the rate of temperature increase was 1 °C/min, and the output of the thermal analysis was finally plotted.

**2.5. Encapsulation Efficiency (EE) and Drug Loading (DL) Capacity of NPs.** Weighed accurately, 2.00 mg NPs in a 2 mL volumetric flask were diluted with acetonitrile to the line, extracted for 15 min with ultrasonic wave, then shook well and filtered. The determination of PTX in the dual-targeted nanoparticles was implemented on an ACQUITY UPLC H-Class System (Waters Corp, Milford, MA, USA), and the DL and EE of the dual-targeted NPs were calculated as follows:

$$\text{DL (\%)} = W_1/W \times 100$$

$$\text{EE (\%)} = W_1/W_2 \times 100$$

where  $W_1$  represents PTX content in NPs,  $W$  indicates total mass of NPs, and  $W_2$  denotes the amount of drug release.

**2.6. Stability Study of PTX@ANG/FA-NPs.** The appropriate amount of PTX@ANG/FA-NPs was taken and dispersed into PBS (pH, 7.4) or 10% FBS, stored at 4 °C for 7 days away from light, and the particle size of the PTX@ANG/FA-NPs was measured daily by a laser diffraction particle size analyzer to observe the time-dependent changes in the particle size.

**2.7. In Vitro Drug Release of ANG/FA-NPs.** The multifunctional probe tested with *in vitro* drug release of PTX from drug-laden NPs was studied by dialysis: 1 mL of PTX@ANG/FA-NPs (PTX concentration = 3.13 mg/mL) was sealed in a dialysis bag [MWCO 3500] and was incubated in 15 mL of phosphate-buffered saline (PBS) at pH 5.0 (simulated intra-

cellular environment of tumor), pH 6.8 (simulated tissue environment of tumor), or pH 7.4 (simulated normal physiological environment), and an appropriate proportion of sodium dodecyl sulfate was added as the dialysis solution. The drug release was investigated and explored at 37 °C with a thermostatic magnetic stirrer rotating at 100 rpm, respectively. After that, 1 mL of dialysate was collected at 15 min, 30 min, 1 h, 2 h, 4 h, 6 h, 8 h, 12 h, 24 h, and 48 h and changed with an equal volume of PBS. The concentrations of collected dialysate were determined with UPLC, and the cumulative amount of PTX released from the dual-targeted NPs was plotted against time.

**2.8. Culture of Cells.** U251, HeLa, and A549 cell lines were fully grown in MEM, Dulbecco's modified Eagle medium (DMEM), and a Roswell Park Memorial Institute (RPMI)-1640 medium, respectively. To stop the microbial activity, supplemented 10% FBS and 1% streptomycin–penicillin were added in the solution and kept at 37 °C in a humidified incubator with 5% CO<sub>2</sub>. All the intermediates and supplements were exchanged every 2 days.

**2.9. In Vitro Cytotoxicity Assay.** To investigate the cytotoxic influence of ANG/FA-NPs, PTX, and PTX@ANG/FA-NPs, U251 cells in a well-digested logarithmic development phase were weakened to  $5 \times 10^4$  cells mL<sup>-1</sup> with MEM comprising 10% FBS, and 100 μL of cell suspension was shifted to a 96-well plate and simmered for 36 h. The cell survival rate was calculated as follows:

$$\text{Cell survival rate (\%)} = \frac{A_{\text{Experimental group}} - A_{\text{Blank group}}}{A_{\text{Control group}} - A_{\text{Blank group}}} \times 100$$

**2.10. Cell Migration Assay.** An *in vitro* scratch wound-healing migration assay was implemented to study cell migration. For this, 70 μL of U251 cell containing media was added to the middle well of the cell insert, and the cells were incubated in an incubator for 24 h. Cells were cultivated in a serum-free MEM for 4 h. The insert was removed with forceps and examined for “scratch” formation using an inverted microscope. If a satisfactory “scratch” could be formed, the cells were washed, and 2 mL of a serum-free medium, containing PTX, ANG/FA-NPs, and PTX@ANG/FA-NPs, was incorporated for incubation. The cells were microscopically visualized at 0, 10, and 24 h in an appropriate field of view, and the proportion of cells that covered the scratched area was calculated under different conditions.

**2.11. Apoptosis Assay.** The cell apoptosis for viability and efficiency of prepared nanomaterials was analyzed by flow cytometry. For this purpose, U251 cells at logarithmic progression periods were collected and immunized uniformly, at an intensity of  $3 \times 10^5$  U251 cells/well, in a 6-well plate, and nursed at 37 °C for 24 h. Next, the cells in the control group were bottled with MEM only, and those in the other groups were treated with suitable concentrations of ANG/FA-NPs and PTX@ANG/FA-NPs. After 48 h of incubation, the cells were gathered and cleaned with cold PBS, centrifuged at 1000 rpm min<sup>-1</sup> for 5 min, the supernatant was cleaned, appropriate amounts of Annexin V-FITC and propidium iodide (PI) stain were supplemented according to the manufacturer's instructions, mixed gently, and the cells were incubated at room temperature for 15 min in the dark, placed in an ice bath, and processed by a flow cytometer.

**2.12. Cellular Uptake Assay.** In this experiment, HeLa, U251, and A549 cells were used to accomplish the uptake assay.

The three cells were inoculated in cell crawlers, respectively, and incubated at 37 °C for 24 h. When the cells were completely adhered, the supernatant was removed, and 20 μg mL<sup>-1</sup> fluorescent nanoparticles were added to the complete medium, containing (RhB@PLGA-NPs, RhB@ANG-NPs, RhB@FA-NPs, and RhB@ANG/FA-NPs), and incubated for 4 h. The cells were then thrice rinsed with prewarmed PBS (pH 7.4; 1 mL each time). After treatment, the cells were stained with Lyso Tracker and 4',6-diamidino-2-phenylindole (DAPI) staining solutions. After staining, the cell crawl was covered on a slide, and the uptake of the cells was observed directly underneath a fluorescence microscope.

**2.13. In Vivo Experiment.** **2.13.1. In Vivo Fluorescence Imaging.** The *in vivo* tissue distributions of dual-targeted PLGA nanoparticles were assessed by a fluorescence imaging system (Bruker, Germany), and BALB/c nude mice were randomized into three groups ( $n = 3/\text{group}$ ): (1) DiR, (2) DiR@FA-NPs, and (3) DiR@ANG/FA-NPs. The free DiR, DiR-loaded FA-NPs, and DiR-loaded ANG/FA-NPs were inoculated into the BALB/c nude mice intravenously (10 mg DiR/kg). At predetermined time points, and mice were anaesthetized and imaged with a fluorescence imaging system. The fluorescence intensity of isolated brains was analyzed to evaluate the brain-targetability of NPs.

**2.13.2. Brain Distribution of PTX@ANG/FA-NPs.** To further confirm that ANG/FA-NPs act as carriers to deliver PTX to the brain, 3 KM mice were injected with PTX@ANG/FA-NPs (50 mg dose of PTX/kg). At predetermined time points, mice were anaesthetized and sacrificed. Brain tissues were quickly collected and homogenized with sterile 0.9% saline (1 g: 2 mL). The homogenate was added with acetonitrile at a ratio of 1:2 to precipitate the protein. After centrifugation of the homogenate at 12 000 rpm at 4 °C for 10 min, the supernatant was concentrated by vacuum centrifugation and 100 μL acetonitrile was added to reconstitute, and then the supernatant was analyzed by ultra-high performance liquid chromatography-quadrupole time-of-flight mass spectrometry (UPLC-Q-TOF-MS).

UPLC-Q-TOF-MS analysis was accomplished on a Waters ACQUITY UPLC system (Waters Corp., Milford, MA, USA) using an ACQUITY UPLC BEH C18 column (1.7 μm, 2.1 mm × 50 mm, Waters Corp., USA) by gradient elution using acetonitrile (A) and 0.1% formic acid in water (B) at a flow rate of 0.3 mL/min. The gradient profile was 0–7 min (A, 60%), 7–7.1 min (A, 60%–20%), 7.1–9 min (A, 20%–60%), then held for 3 min. The injection volume was 2 μL. The temperature of the column oven was set to 30 ± 5 °C. Mass spectrometry was carried out using a TOF-MS system (Waters Corp., Milford, MA, USA) fitted with an electrospray ionization (ESI) ion source. Ionization was performed in the positive electrospray mode. The MS parameters were as follows: capillary voltage, 3 kV; cone voltage, 40 V; source temperature, 120 °C; cone gas flow, 50 L/h; desolvation gas temperature, 400 °C; desolvation gas flow, 700 L/h; collision energy, 6 V. The TOF-MS data were attained in centroid mode over the  $m/z$  range of 50–1200 Da with a scan rate of 0.2 s and an interscan delay of 0.02 s.

**2.13.3. Statistical Analysis.** Experimental data were taken as mean ± standard deviation (SD). The *t* test and one-way ANOVA followed by Dunnett's tests were used to perform statistical analysis, where *P*-values < 0.05 (\*) and *P*-values < 0.01 (\*\*\*) were considered statistically significant.

### 3. RESULTS AND DISCUSSION

The overall tailoring of multifunctional hybrid nanostructure, their characterization, and evaluation *in vitro/in vivo* therapeutics have been performed for gliomas through the blood–brain barrier as summarized in schematic Figure 1.

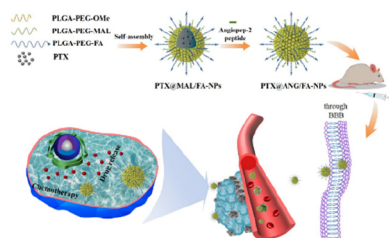


**Figure 1.** Schematic illustration of therapeutic efficiency of multifunctional hybrid nanostructure against blood–brain barrier gliomas.

**3.1. Characterization of PTX@ANG/FA-NPs.** The prepared PTX@ANG/FA-NPs were characterized initially via scattering mechanism under laser-beam irradiation, and a bright “channel” could be observed in the solution of PTX@ANG/FA-NPs, indicating a promising Tyndall effect, see Figure 2(a). This is a new nanosensing method for naïve, subtle, definite, visual detection of PTX@ANG/FA-NPs that showed better result compared to a previous one.<sup>34,35</sup> Then TEM exhibited sphere or similar spherical morphologies with diameters 100–200 nm in aqueous sodium cholate solution as shown in Figure 2(b). The morphology was novel and ideal for drug delivery. The size of PTX@ANG/FA-NPs was  $157.9 \pm 3.1$  nm and zeta potential was  $-7.35 \pm 3.8$  mV via size analyzers and particle size distribution as shown in Figure 2(c). The small size NPs and low zeta potential showed high stability and suitability for current studies. In the early reports, small size nanomaterials, stable structure, and being biodegradable were found to be suitable for delivery systems.<sup>36,37</sup>

**3.2. Stability of PTX@ANG/FA-NPs.** For assessment regarding the efficiency of functional probes, the stability is key factor for proper functioning of nanomaterials. For this purpose, the volume of residual ANG in the supernatant solution was quantified via a BCA protein concentration by using standard method, and it was found that the grafting rate of ANG was equal to 63.9%, which is highly feasible for diagnosis of diseases like cancer.<sup>38,39</sup> However, when samples underwent phase changes or chemical reaction, they absorbed and emitted heat, and the glass transition temperature may have accordingly changed that was detected by DSC. The glass transition temperatures of ANG and FA-PLGA-NPs were found to be 29.84 and 34.16 °C, respectively, while ANG/FA-PLGA-NPs showed two peaks in the graph with the glass transition temperatures of 33.14 °C (ANG) and 36.89 °C (FA-PLGA). Hence, it could be concluded that the ANG reacted with PLGA chemically Figure 3(a). The current materials are suggested to be effective for all kinds of hydrophobic drugs for effective treatment.<sup>40,41</sup>

The encapsulation efficiency (EE) and drug loading (DL) of PTX@ANG/FA-NPs were also very important for successful target delivery in *in vitro* and *in vivo*. The EE and DL of PTX@ANG/FA-NPs were found to be  $49.0 \pm 1.79\%$  and  $5.9 \pm 0.8\%$ , respectively. Moreover, it has also been observed that *in vitro*, slow discharge of drug behavior was evaluated in three PBS solutions at different pH (7.4, 6.8, and 5.0) according to the *in vitro* drug release curve.<sup>42,43</sup> The highest amount of release of dual-targeted NPs was recorded at a pH of 5.0, which could reach 42% after 72 h. The results suggest that the dual-targeted PLGA nanoparticles have the possibility of pH-responsive release Figure 3(b). The most important factor is how a functional probe was stabilized; therefore, the stability of PTX@ANG/FA-NPs is indicated in Figure 3(c). The average particle size of PTX@ANG/FA-NPs maintained in PBS or 10% FBS was  $\sim 160$ – $170$  nm for 7 days, and less significant differences were found.

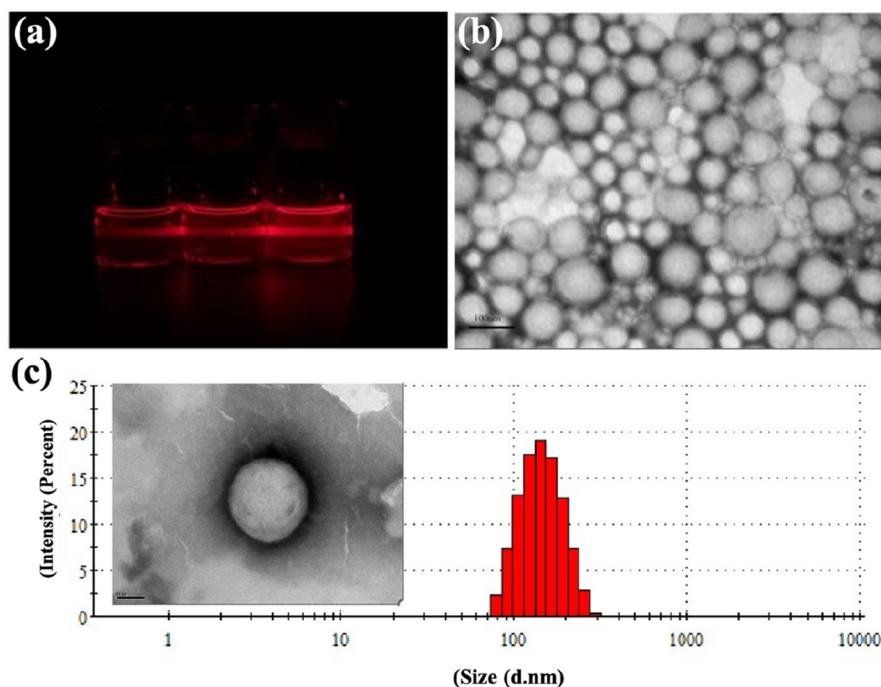


**Figure 2.** Characterization of PTX@ANG/FA-NPs. (a) Tindal effect, (b) TEM images, (c) particle size distribution.

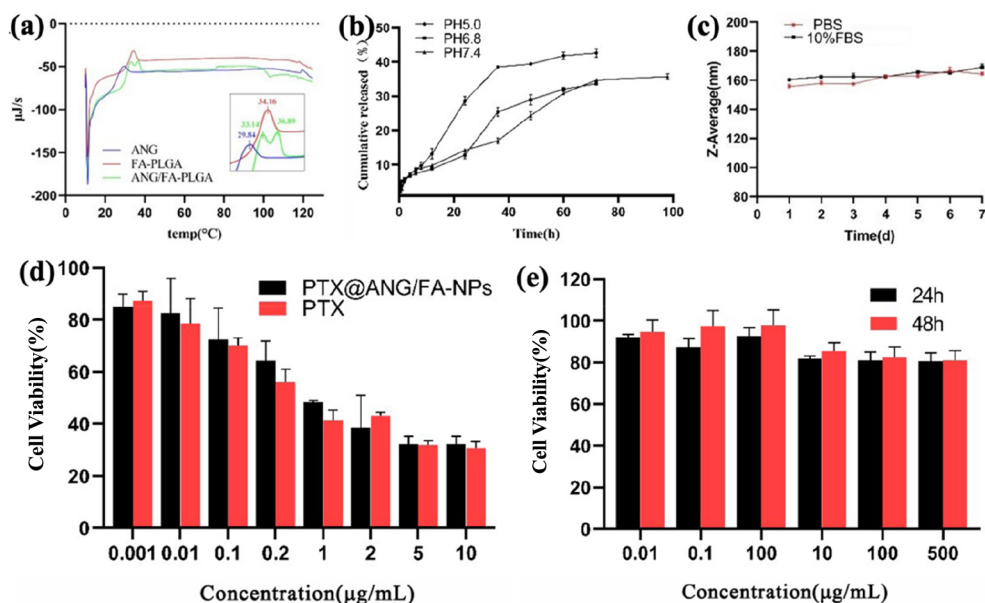


**Figure 3.** Stability and cytotoxicity illustration of ANG, FA-PLGA-NPs, and ANG/FA-NPs. (a) Stability test, (b, c) cumulative release profiles of dual-targeted nanoparticles in three media at pH of 5.0, 6.8, and 7.4, respectively, (c) viability and cytotoxicity of PTX@ANG/FA-NPs, (d) viability of U251 cells treated with PTX and PTX@ANG/FA-NPs, (e) time point.

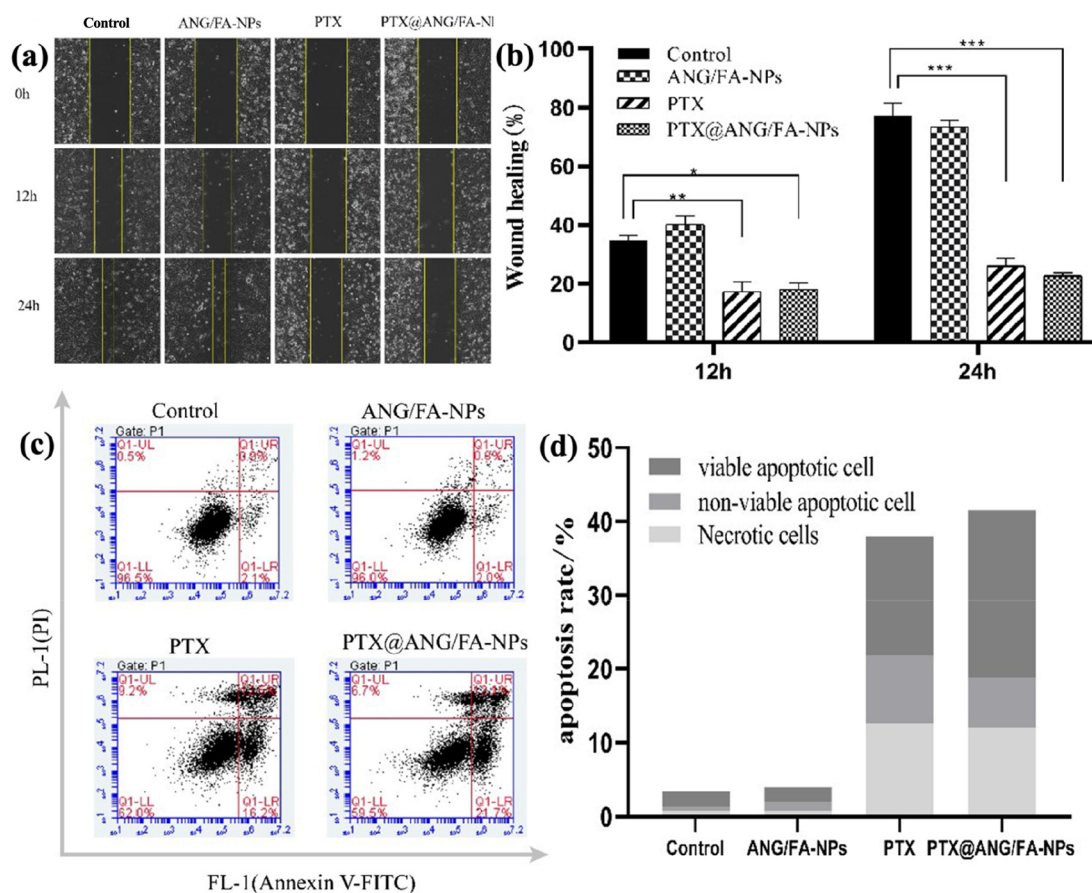


**Figure 4.** (a) Images of scratch assay of cells collected at 0, 12, and 24 h. (b) Quantitative assessment of wound healing rate. (c) Apoptosis of U251 cells was induced by ANG/FA-NPs, PTX, and PTX@ANG/FA-NPs. (d) Quantitative results of the apoptosis assay of U251 cells subjected to different drugs (\* $P < 0.05$ , \*\* $P < 0.01$ , \*\*\* $P < 0.001$ ).

**3.3. Cytotoxicity of PTX@ANG/FA-NPs.** The biocompatibility of materials is very important; therefore, the prepared structure needs to be free of toxicity for the normal cell to be an

ideal vector for drug delivery. As shown in Figure 3(d), it can be concluded that both PTX and PTX@ANG/FA-NPs can prevent the multiplying of U251 cells in a dose-dependent manner with

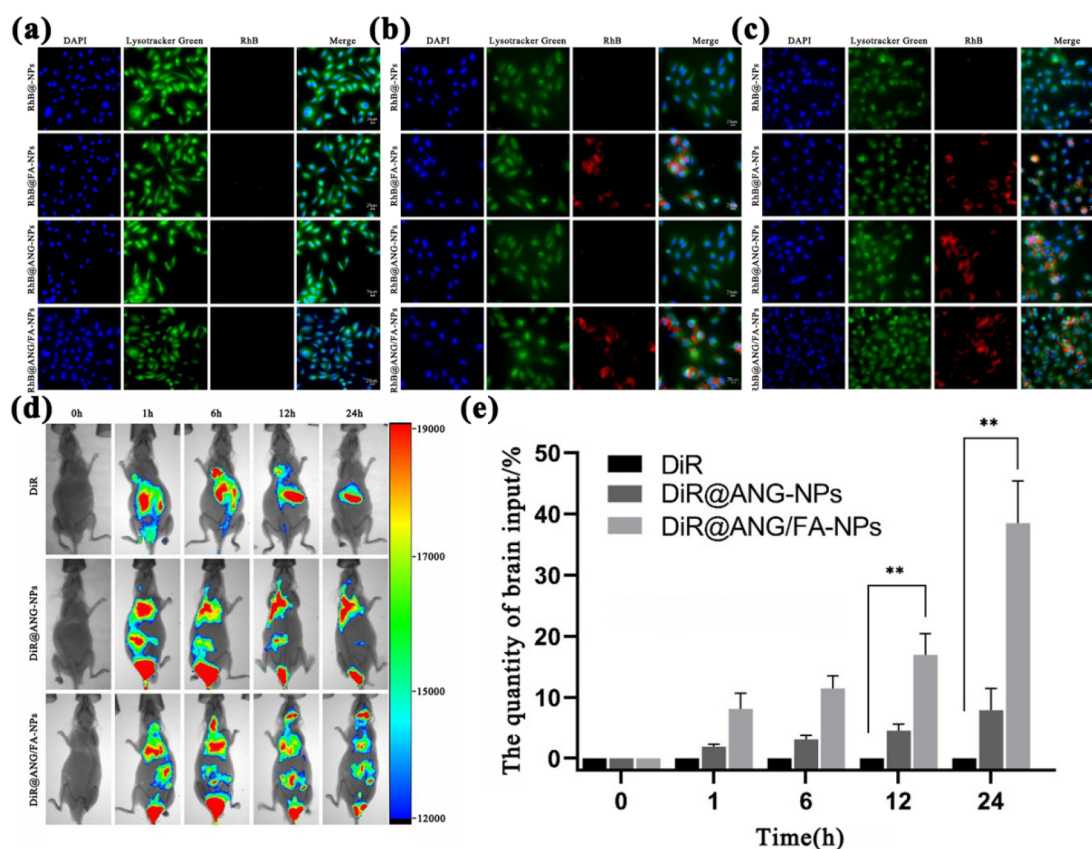


**Figure 5.** Illustration of uptake of RhB@PLGA-NPs, RhB@FA-PLGA-NPs, RhB@ANG-PLGA-NPs, and RhB@ANG/FA-NPs by (a) A549, (b) HeLa, and (c) U251 cells, respectively (partially quoted from a previously published article<sup>53</sup>). (d) *In vivo* imaging of BALB/c-nu mice after intravenous injection of nanoparticles. (e) Quantity of DiR crossing BBB ( $n = 3$ ,  $**p < 0.01$ ).

respect to time. The half maximal inhibitory concentration ( $IC_{50}$ ) values of PTX@ANG/FA-NPs and PTX were 1.07 and 1.27  $\mu\text{g}/\text{mL}$ , respectively. The repressive influence of PTX@ANG/FA-NPs on U251 cells was 1.2-times that of PTX. The cell counting kit-8 (CCK-8) was employed initially to verify the biosafety of the ANG/FA-NPs, and the results are displayed in Figure 3(e). After incubation of U251 cells with ANG/FA-NPs at an intensity of 500  $\mu\text{g}/\text{mL}$  for 24 and 48 h, the cell sustainability reached more than 80%, which indicated the low toxicity and biosafety of ANG/FA-NPs. This can be related to the easy uptake of targeted nanodrugs by tumor cells; on the one hand, the slow-release nature of the materials increased the release of drugs in tumor cells, thereby highlighting a greater antitumor capability of PTX@ANG/FA-NPs. These novel results confirmed the validation of the previous work as nanomaterials delivery of drug and can be used for multiple applications.<sup>44–46</sup>

**3.4. Cell Migration and Apoptosis Assay.** The capacity of tumor cells to enter and migrate is the most basic biological characteristic of malignant tumors, and the cell scratch test is a simple method to detect the passage capacity of tumor cells. The results showed that the treatment group without administration of ANG/FA-NPs had almost no inhibitory effect on U251 cells compared with the control group, indicating that ANG/FA-NPs were essentially nontoxic to the cells Figure 4(a).

Both PTX and PTX@ANG/FA-NPs had shown very effective and significant inhibitory effects on healing of U251 cells. These results showed that our carrier system was successful and very useful for hydrophobic drugs. It has been observed that the

cellular healing rates of PTX and PTX@ANG/FA-NPs at 24 h were 26.1% and 22.5%, respectively Figure 4(b). Although both groups could significantly reduce the migration ability of U251 cells, the PTX@ANG/FA-NPs were more applicable in inhibiting the passage of U251 cells than PTX. This may be related to the ability of the PTX@ANG/FA-NPs to sustain the release of PTX, confirming a great ability of PTX@ANG/FA-NPs to inhibit the migration of tumor cells. Quantitative analysis was also carried out and estimated the positive effect of nanomaterials efficiency for delivery as Figure 4(b). Furthermore, the cell death measurements were very important, especially the cell cycle stages that determine the cell cycle phases and their functionality. To see this effect, flow cytometry was used to compare the cancer cell apoptosis capability of PTX, ANG/FA-NPs, and PTX@ANG/FA-NPs. According to the results of flow cytometry, the rates of cell apoptosis for ANG/FA-NPs, PTX, and PTX@ANG/FA-NPs were 3.2%, 25.2%, and 28.4%, respectively. It showed that ANG/FA-NPs did not promote the cell apoptosis and were basically nontoxic compared with the control group. Both PTX and PTX@ANG/FA-NPs could successfully stimulate apoptosis of U251 cells. However, compared with PTX, the apoptotic capability of PTX@ANG/FA-NPs was greater, and the results of the apoptosis assay were steady with those of the cell scrape assay for the determination process. It is noteworthy that the PTX@ANG/FA-NPs were more easily taken up by tumor cells, confirming their stronger apoptotic effects in term of quantitative analysis Figure 4(c,d). This will also help researchers to explore the functional role of the prepared

probe, which is far better as compared to results in literature reports.<sup>47–49</sup>

**3.5. Cellular Uptake Assay.** Human glioblastoma U251 cells and human cervical cancer HeLa cells are folate receptor positive,<sup>50,51</sup> while there are no folate receptor on human lung cancer A549 cells;<sup>52</sup> therefore, here we can detect FA graft on the PLGA. LRP1 is communicated on the BBB and contributes in the moving of endogenous ligands from blood to brain. As ANG is the ligand of LRP1 and has been widely used as brain delivery vector due to their superior transcytosis facility across the BBB. U251 cells are LRP1 positive, while no expression on human cervical cancer HeLa cells and human lung cancer A549 cells was observed. In the field of the fluorescence microscope, RhB appear in red, nucleus (DAPI stain) appears in blue, and cytoplasm (LysoTracker stain) appears in green. Scale bars are 20  $\mu\text{m}$  Figure 5(a–c). We observed that RhB@PLGA-NPs, RhB@FA-PLGA-NPs, RhB@ANG-PLGA-NPs, and RhB@ANG/FA-NPs were barely taken up by A549 cells as shown in Figure 5(a). The results illustrated that the four nanoparticles were not engulfed because folate receptor and LRP1 showed low expression on A549 cells. HeLa cell lines had more folate receptors on their surface, which underwent specific uptake with NPs containing folate on their surface. Figure 5(b) shows that RhB@FA-PLGA-NPs and RhB@ANG/FA-NPs emitted a significant red fluorescence in HeLa cells, while RhB@PLGA-NPs and RhB@ANG-PLGA-NPs were not largely engulfed. U251 cells are LRP1 and FRs positive, and as depicted in Figure 5(c), a good uptake of RhB@FA-PLGA-NPs, RhB@ANG-PLGA-NPs, and RhB@ANG/FA-NPs in U251 cells could be observed, while the NPs were mainly distributed in the cytoplasm of tumor cells after uptake. The current work showed very effective and significant results of prepared ANG/FA-NPs as compared to control in all kinds of cancer cells. However, the previous reports and current reports match the result but with ANG/FA-NPs showing more stability and durability.<sup>52</sup>

**3.6. In Vivo Fluorescence Imaging.** To estimate nanodrug delivery effectiveness, *in vivo* distribution of dual-modified NPs in tissue, free DiR, DiR-loaded FA-NPs, and ANG/FA-NPs were prepared for *in vivo* imaging on the BALB/c nude mice. As Figure 5(d) indicated, free DiR, DiR@FA-NPs and DiR@ANG/FA-NPs were well distributed in liver. Free DiR had no distribution into the brain until 24 h after administration, whereas the distribution of DiR@FA-NPs and DiR@ANG/FA-NPs gradually increased in the brain 1 h after administration. However, the distribution of DiR@ANG/FA-NPs was significantly stronger than that of DiR@FA-NPs, indicating that the dual-modified NPs had strong efficacy in brain targeting.

*In vivo* imaging of BALB/c-nu mice after intravenous injection of DiR@ANG/FA-NPs was represented in Figure 5(d), where a significant quantity of peptides crossed the blood–brain barrier. Overall, our current findings fully explain that the *in vivo* fluorescence imaging provides a visual, rapid, and reliable procedure as compared to the traditional approaches such as real-time quantitative PCR in identifying cancer.

From Figure 5(d), there were different time points from 0 to 24 h with our functional probes, DiR, DiR@ANG, and DiR@ANG/FA NPs that were investigated, and the % efficiency was significantly enhanced from our prepared materials. Currently, very less or few reports are available to completed glioma mice for brain-targeted drug delivery and treatment; because the modeling of glioma mice had serious difficulties, the follow-up test results will be reported with the animal pharmacological experiments. The *in vivo*, comprising active cells and the

complete body, was important for efficient tracking of nanoparticles, as DiR is a cytomembrane fluorescent probe and is widely used for *in vivo* fluorescence imaging of small animals. In our studies, the results of imaging experiments revealed that DiR@ANG/FA-NPs had a greater ability to accumulate at sites of tumor BBB disruption. To confirm that ANG/FA-NPs helped in delivering PTX to the brain, PTX distribution in the brain was analyzed by UPLC-Q-TOF-MS, as shown in Figure S1, whereas PTX was detected in the brain of PTX@ANG/FA-NPs treated mice.

## 4. CONCLUSIONS

In the present study, PTX@ANG/FA-NPs showed good biocompatibility and a highly significant antitumor activity. The structural and morphological characterization of PTX@ANG/FA-NPs showed a highly stable and narrow size of 160 to 170 nm as effective carrier. The enhanced results *in vitro*, during cellular activities of the ANG/FA-NPs, PTX, and PTX@ANG/FA-NPs, were almost nontoxic, indicating that the ANG/FA-NPs had an acceptable biocompatibility. The flow cytometry results also support that the ANG/FA-NPs group cannot promote the apoptosis of U251 cells, while PTX@ANG/FA-NPs exhibited a stronger ability to enhance the apoptosis than PTX. *In vivo* results showed that incorporation of PTX into ANG/FA-NPs achieved better brain-targeted delivery of PTX for the cure of glioblastomas. The imaging and *in vitro* results showed efficiency of the nanodrug delivery system.

The results indicated that the PTX dual-target nanoparticles have the ability to cross the BBB and target glioblastoma cells, split as a prospective candidate in future of drug progression. The novel nanodrug distribution system also enhanced the distribution of drugs and biological therapeutics for glioblastomas.

## ■ ASSOCIATED CONTENT

### SI Supporting Information

The Supporting Information is available free of charge at <https://pubs.acs.org/doi/10.1021/acsomega.2c08265>.

Additional experimental materials, grafting rate of peptides and UPLC-MS extracted ion chromatograms of PTX (PDF)

## ■ AUTHOR INFORMATION

### Corresponding Authors

Dewen Liu – Institute of Chinese Materia Medica, China Academy of Chinese Medical Sciences, Beijing 10700, China; Email: [dwliu@icmm.ac.cn](mailto:dwliu@icmm.ac.cn)

Jinyu Wang – Institute of Chinese Materia Medica, China Academy of Chinese Medical Sciences, Beijing 10700, China; Email: [jinyu024@163.com](mailto:jinyu024@163.com)

### Authors

Zemin Ou – Institute of Chinese Materia Medica, China Academy of Chinese Medical Sciences, Beijing 10700, China; [orcid.org/0000-0003-2719-0548](https://orcid.org/0000-0003-2719-0548)

Xinjian Li – Institute of Chinese Materia Medica, China Academy of Chinese Medical Sciences, Beijing 10700, China

Yun You – Institute of Chinese Materia Medica, China Academy of Chinese Medical Sciences, Beijing 10700, China

Complete contact information is available at:

<https://pubs.acs.org/doi/10.1021/acsomega.2c08265>

## Author Contributions

<sup>‡</sup>Z.M.O. and X.J.L. contributed equally to this work. Z.M.O., X.J.L., and J.Y.W. conceived the project. Z.M.O., X.J.L., J.Y.W., and Y.Y. performed the experiments. D.W.L. and X.J.L. performed the characterization of NPs and analyzed the data. Z.M.O. and X.J.L. wrote the manuscript. All authors discussed the data and commented on the manuscript.

## Notes

The authors declare no competing financial interest.

## ACKNOWLEDGMENTS

This work was supported by Outstanding Young Science and Technology Talent Project of China Academy of Chinese Medical Sciences (ZZ14-YQ-024) and Scientific and technological innovation project of China Academy of Chinese Medical Sciences (C12021A04303).

## REFERENCES

- (1) Ostrom, Q. T.; Gittleman, H.; Farah, P.; Ondracek, A.; Chen, Y.; Wolinsky, Y.; Stroup, N. E.; Kruchko, C.; Barnholtz-Sloan, J. S. CBTRUS statistical report: Primary brain and central nervous system tumors diagnosed in the United States in 2006–2010. *Neuro Oncol* **2013**, *15* (2), 1–56.
- (2) Ostrom, Q. T.; Cioffi, G.; Waite, K.; Kruchko, C.; Barnholtz-Sloan, J. S. CBTRUS Statistical Report: Primary Brain and Other Central Nervous System Tumors Diagnosed in the United States in 2014–2018. *Neuro Oncol* **2021**, *23* (12), 1–105.
- (3) Jain, V.; Jain, S.; Mahajan, S. C. Nanomedicines based drug delivery systems for anti-cancer targeting and treatment. *Curr. Drug Deliv* **2015**, *12* (2), 177–191.
- (4) Rajaratnam, V.; Islam, M. M.; Yang, M.; Slaby, R.; Ramirez, H. M.; Mirza, S. P. Glioblastoma: Pathogenesis and Current Status of Chemotherapy and Other Novel Treatments. *Cancers (Basel)* **2020**, *12* (4), 11–23.
- (5) Geribaldi-Doldán, N.; Fernández-Ponce, C.; Quiroz, R. N.; Sánchez-Gomar, I.; Escorcía, L. G.; Velásquez, E. P.; Quiroz, E. N. The Role of Microglia in Glioblastoma. *Front Oncol* **2021**, *10* (3), 60–34.
- (6) Tang, W.; Fan, W.; Lau, J.; Deng, L.; Shen, Z.; Chen, X. Emerging blood-brain-barrier-crossing nanotechnology for brain cancer therapeutics. *Chem. Soc. Rev.* **2019**, *48* (11), 2967–3014.
- (7) Liu, W. J.; Yin, Y. B.; Sun, J. Y.; Feng, S.; Ma, J. K.; Fu, X. Y.; Hou, Y. J.; Yang, M. F.; Sun, B. L.; Fan, C. D. Natural borneol is a novel chemosensitizer that enhances Temozolomide-induced anticancer efficiency against human glioma by triggering mitochondrial dysfunction and reactive oxide species-mediated oxidative damage. *Onco Targets Ther* **2018**, *11* (5), S429–S439.
- (8) Zhao, F.; Zhong, L.; Luo, Y. Endothelial glycocalyx as an important factor in composition of blood-brain barrier. *CNS Neurosci Ther* **2021**, *27* (1), 26–35.
- (9) Saint-Pol, J.; Gosselet, F.; Duban-Deweert, S.; Pottiez, G.; Karamanos, Y. Targeting and Crossing the Blood-Brain Barrier with Extracellular Vesicles. *Cells* **2020**, *9* (4), 55–71.
- (10) Huang, X.; Hussain, B.; Chang, J. Peripheral inflammation and blood-brain barrier disruption: effects and mechanisms. *CNS Neurosci Ther* **2021**, *27* (1), 36–47.
- (11) Kadry, H.; Noorani, B.; Cucullo, L. A blood-brain barrier overview on structure, function, impairment, and biomarkers of integrity. *Fluids Barriers CNS* **2020**, *17* (1), 69.
- (12) Ruan, S.; Zhou, Y.; Jiang, X.; Gao, H. Rethinking CRITID Procedure of Brain Targeting Drug Delivery: Circulation, Blood Brain Barrier Recognition, Intracellular Transport, Diseased Cell Targeting, Internalization, and Drug Release. *Adv. Sci. (Weinh)* **2021**, *8* (9), 2004025.
- (13) Jena, L.; Mcerlean, E.; Mccarthy, H. Delivery across the blood-brain barrier: nanomedicine for glioblastoma multiforme. *Drug Deliv Transl Res.* **2020**, *10* (2), 304–318.
- (14) Cai, Z.; Qiao, P. F.; Wan, C. Q.; Cai, M.; Zhou, N. K.; Li, Q. Role of Blood-Brain Barrier in Alzheimer's Disease. *J. Alzheimers Dis* **2018**, *63* (4), 1223–1234.
- (15) Parker, A.; Fonseca, S.; Carding, S. R. Gut microbes and metabolites as modulators of blood-brain barrier integrity and brain health. *Gut Microbes* **2020**, *11* (2), 135–157.
- (16) Pardridge, W. M. Blood-brain barrier drug targeting: the future of brain drug development. *Mol. Interv* **2003**, *3* (2), 90–105.
- (17) Pardridge, W. M. Blood-brain barrier biology and methodology. *J. Neurovirol* **1999**, *5* (6), 556–569.
- (18) Gao, H. Perspectives on Dual Targeting Delivery Systems for Brain Tumors. *J. Neuroimmune Pharmacol* **2017**, *12* (1), 6–16.
- (19) Lv, F.; Hasan, M.; Dang, H.; Hassan, S. G.; Meng, W. W.; Deng, Y. L.; Dai, R. J. Optimized Luteolin Loaded Solid Lipid Nanoparticle Under Stress Condition for Enhanced Bioavailability in Rat Plasma. *J. Nanosci Nanotechnol* **2016**, *16* (9), 9443–9449.
- (20) Dang, H.; Meng, M. H. W.; Zhao, H. W.; Iqbal, J.; Dai, R. J.; Deng, Y. L.; Lv, F. Luteolin-loaded solid lipid nanoparticles synthesis, characterization, & improvement of bioavailability, pharmacokinetics in vitro and vivo studies. *J. Nanopart. Res.* **2014**, *16* (4), 10.
- (21) Luo, F.; Wang, M.; Huang, L.; Wu, Z.; Wang, W.; Zafar, A.; Tian, Y.; Hasan, M.; Shu, X. Synthesis of Zinc Oxide Eudragit FS30D Nanohybrids: Structure, Characterization, and Their Application as an Intestinal Drug Delivery System. *ACS Omega* **2020**, *5* (20), 11799–11808.
- (22) Hasan, M.; Iqbal, J.; Awan, U.; Xin, N.; Dang, H.; Waryani, B.; Saeed, Y.; Ullah, K.; Rongji, D.; Deng, Y. LX loaded nanoliposomes synthesis, characterization and cellular uptake studies in H2O2 stressed SH-SY5Y cells. *J. Nanosci Nanotechnol* **2014**, *14* (6), 4066–4071.
- (23) Li, Y.; Liao, C.; Tjong, S. C. Synthetic Biodegradable Aliphatic Polyester Nanocomposites Reinforced with Nanohydroxyapatite and/or Graphene Oxide for Bone Tissue Engineering Applications. *Nanomaterials (Basel)* **2019**, *9* (4), 233–245.
- (24) Bonacucina, G.; Perinelli, D. R.; Cespi, M.; Palmieri, G. F. PEGylated polylactide (PLA) and poly (lactic-co-glycolic acid) (PLGA) copolymers for the design of drug delivery systems. *Journal of Pharmaceutical Investigation* **2019**, *49* (4), 443–458.
- (25) Makadia, H. K.; Siegel, S. J. Poly Lactic-co-Glycolic Acid (PLGA) as Biodegradable Controlled Drug Delivery Carrier. *Polymers (Basel)* **2011**, *3* (3), 1377–1397.
- (26) Kolska, Z.; Valha, P.; Slepicka, P.; Svorcik, V. Refractometric study of systems water-poly (ethylene glycol) for preparation and characterization of Au nanoparticles dispersion. *Arab J. Chem.* **2019**, *12* (8), S019–S027.
- (27) Meunier, M.; Goupil, A.; Lienard, P. Predicting drug loading in PLA-PEG nanoparticles. *Int. J. Pharm.* **2017**, *526* (1–2), 157–166.
- (28) Na, D. H.; Emami, F.; Yazdi, S. J. M. Poly(lactic acid)/poly(lactic-co-glycolic acid) particulate carriers for pulmonary drug delivery. *Journal of Pharmaceutical Investigation* **2019**, *49* (4), 427–442.
- (29) Ruan, S.; Yuan, M.; Zhang, L.; Hu, G.; Chen, J.; Cun, X.; Zhang, Q.; Yang, Y.; He, Q.; Gao, H. Tumor microenvironment sensitive doxorubicin delivery and release to glioma using angiopep-2 decorated gold nanoparticles. *Biomaterials* **2015**, *37* (4), 425–435.
- (30) Kuo, Y. C.; Chen, Y. C. Targeting delivery of etoposide to inhibit the growth of human glioblastoma multiforme using lactoferrin- and folic acid-grafted poly(lactide-co-glycolide) nanoparticles. *Int. J. Pharm.* **2015**, *479* (1), 138–149.
- (31) Demeule, M.; Currie, J. C.; Bertrand, Y.; Ché, C.; Nguyen, T.; Régina, A.; Gabathuler, R.; Castaigne, J. P.; Béliveau, R. Involvement of the low-density lipoprotein receptor-related protein in the transcytosis of the brain delivery vector angiopep-2. *J. Neurochem* **2008**, *106* (4), 1534–1544.
- (32) Harshita; Barkat, M. A.; Beg, S.; Pottoo, F. H.; Ahmad, F. J. Nanopaclitaxel therapy: an evidence based review on the battle for next-generation formulation challenges. *Nanomedicine (Lond)* **2019**, *14* (10), 1323–1341.
- (33) Sofias, A. M.; Dunne, M.; Storm, G.; Allen, C. The battle of "nano" paclitaxel. *Adv. Drug Deliv Rev.* **2017**, *122* (34), 20–30.

- (34) Yan, H.; You, Y.; Li, X.; Liu, L.; Guo, F.; Zhang, Q.; Liu, D.; Tong, Y.; Ding, S.; Wang, J. Preparation of RGD Peptide/Folate Acid Double-Targeted Mesoporous Silica Nanoparticles and Its Application in Human Breast Cancer MCF-7 Cells. *Front Pharmacol* **2020**, *11* (3), 898.
- (35) Sun, Y.; Yuan, K.; Mo, X.; Chen, X.; Deng, Y.; Liu, C.; Yuan, Y.; Nie, J.; Zhang, Y. Tyndall-Effect-inspired assay with gold nanoparticles for the colorimetric discrimination and quantification of mercury ions and glutathione. *Talanta* **2022**, *238* (1), 122.
- (36) Hong, W.; Guo, F.; Yu, N.; Ying, S.; Lou, B.; Wu, J.; Gao, Y.; Ji, X.; Wang, H.; Li, A.; Wang, G.; Yang, G. A Novel Folic Acid Receptor-Targeted Drug Delivery System Based on Curcumin-Loaded  $\beta$ -Cyclodextrin Nanoparticles for Cancer Treatment. *Drug Des Devel Ther* **2021**, *15* (7), 2843–2855.
- (37) Helmy, S. A.; El-Mofty, S.; El Gayar, A. M.; El-Sherbiny, I. M.; El-Far, Y. M. Novel doxorubicin/folate-targeted trans-ferulic acid-loaded PLGA nanoparticles combination: In-vivo superiority over standard chemotherapeutic regimen for breast cancer treatment. *Biomed Pharmacother* **2022**, *145* (12), 112–123.
- (38) Sarangdhar, M. A.; Allam, R. Angiogenin (ANG)-Ribonuclease Inhibitor (RNH1) System in Protein Synthesis and Disease. *Int. J. Mol. Sci.* **2021**, *22* (3), 337–342.
- (39) Machado, J. S R.; Machado, M S R.; Bertagnolli, T. V.; Martins, L a B.; Freitas, S. F.; Ovidio, P. P.; Sandrim, V. C.; Cardoso, V. C.; Bettiol, H.; Barbieri, M. A.; Cavalli, R. C. Role of plasma PIGF, PDGF-AA, ANG-1, ANG-2, and the ANG-1/ANG-2 ratio as predictors of preeclampsia in a cohort of pregnant women. *Pregnancy Hypertens* **2019**, *16* (21), 105–111.
- (40) Luo, F.; Zeng, D.; Chen, R.; Zafar, A.; Weng, L.; Wang, W.; Tian, Y.; Hasan, M.; Shu, X. PEGylated dihydromyricetin-loaded nanoliposomes coated with tea saponin inhibit bacterial oxidative respiration and energy metabolism. *Food Funct* **2021**, *12* (19), 9007–9017.
- (41) Liu, N.; Park, H. J. Factors effect on the loading efficiency of Vitamin C loaded chitosan-coated nanoliposomes. *Colloids Surf. B Biointerfaces* **2010**, *76* (1), 16–19.
- (42) Hasan, M.; Zafar, A.; Yousaf, M.; Gulzar, H.; Mehmood, K.; Hassan, S. G.; Saeed, A.; Yousaf, A.; Mazher, A.; Rongji, D.; Mahmood, N. Synthesis of Loureirin B-Loaded Nanoliposomes for Pharmacokinetics in Rat Plasma. *ACS Omega* **2019**, *4* (4), 6914–6922.
- (43) Lizundia, E.; Armentano, I.; Luzi, F.; Bertoglio, F.; Restivo, E.; Visai, L.; Torre, L.; Puglia, D. Synergic Effect of Nanolignin and Metal Oxide Nanoparticles into Poly(l-lactide) Bionanocomposites: Material Properties, Antioxidant Activity, and Antibacterial Performance. *ACS Appl. Bio Mater.* **2020**, *3* (8), 5263–5274.
- (44) Song, Y. Y.; Yuan, Y.; Shi, X.; Che, Y. Y. Improved drug delivery and anti-tumor efficacy of combinatorial liposomal formulation of genistein and plumbagin by targeting Glut1 and Akt3 proteins in mice bearing prostate tumor. *Colloids Surf. B Biointerfaces* **2020**, *190* (34), 110–137.
- (45) Seifu, M. F.; Nath, L. K.; Dutta, D. Hyaluronic acid-docetaxel conjugate loaded nanoliposomes for targeting tumor cells. *International Journal of Applied Pharmaceutics* **2020**, *34* (2), 88–99.
- (46) Al-Samydai, A.; Alshaer, W.; Al-Dujaili, E a S.; Azzam, H.; Aburjai, T. Preparation, Characterization, and Anticancer Effects of Capsaicin-Loaded Nanoliposomes. *Nutrients* **2021**, *13* (11), 117–135.
- (47) Wu, X. H.; Yao, L. T.; Al-Baadani, M. A.; Ping, L. C.; Wu, S. Y.; Al-Bishari, A. M.; Hiiruyie, K.; Deng, Z. N.; Liu, J. S.; Shen, X. K. Preparation of multifunctional drug sustained-release system by atomic layer deposition of ZnO in mesoporous titania coating. *Ceram. Int.* **2020**, *46* (7), 9406–9414.
- (48) Wang, Z.; Song, X.; Yang, H.; Maimaitiaili, A.; Wang, T. Development and in vitro characterization of rifapentine microspheres-loaded bone implants: a sustained drug delivery system. *Ann. Palliat Med.* **2020**, *9* (2), 375–387.
- (49) Mondal, S.; Hoang, G.; Manivasagan, P.; Moorthy, M. S.; Phan, T. T. V.; Kim, H. H.; Nguyen, T. P.; Oh, J. Rapid microwave-assisted synthesis of gold loaded hydroxyapatite collagen nano-bio materials for drug delivery and tissue engineering application. *Ceram. Int.* **2019**, *45* (3), 2977–2988.
- (50) Nwahara, N.; Abrahams, G.; Prinsloo, E.; Nyokong, T. Folic acid-modified phthalocyanine-nanozyme loaded liposomes for targeted photodynamic therapy. *Photodiagnosis Photodyn Ther* **2021**, *36* (9), 102–126.
- (51) Wang, X.; Tu, M.; Tian, B.; Yi, Y.; Wei, Z.; Wei, F. Synthesis of tumor-targeted folate conjugated fluorescent magnetic albumin nanoparticles for enhanced intracellular dual-modal imaging into human brain tumor cells. *Anal. Biochem.* **2016**, *512* (17), 8–17.
- (52) Liu, F.; Chen, Y.; Li, Y.; Guo, Y.; Cao, Y.; Li, P.; Wang, Z.; Gong, Y.; Ran, H. Folate-receptor-targeted laser-activable poly(lactide-co-glycolic acid) nanoparticles loaded with paclitaxel/indocyanine green for photoacoustic/ultrasound imaging and chemo/photothermal therapy. *Int. J. Nanomedicine* **2018**, *13* (9), 5139–5158.
- (53) Li, X. J.; You, Y.; Zhang, Q. L.; Zhang, B. B.; Yan, L.; Ou, Z. M.; Zhang, Y.; Wang, Y. J.; Tong, Y.; Liu, D. W.; Wang, J. Y. Preparation of paclitaxel-loaded and folic acid-modified poly (lactic-co-glycolic acid) nano-micelles and in vitro anticancer effect on cervical cancer HeLa cells. *Zhongguo Zhong Yao Za Zhi* **2021**, *46* (10), 2481–2488.